



Strain-Amplified Exciton Chirality in Organic-Inorganic Hybrid MaterialsJin Xiao,¹ Haofeng Zheng,¹ Yanan Liu,¹ Li Fang^{1,2},,² Jing Li,³ Jongchan Kim,⁴ Yanlong Wang,¹
Qi Liu,¹ Xuyu Ma,¹ and Shaocong Hou^{1,5,*}¹*School of Electrical Engineering and Automation, Wuhan University, Wuhan 430072, People's Republic of China*²*School of Science, Hubei University of Technology, Wuhan 430068, People's Republic of China*³*Key Laboratory of Photochemical Conversion and Optoelectronic Materials, Technical Institute of Physics and Chemistry, Chinese Academy of Sciences, Beijing 100190, People's Republic of China*⁴*Department of Integrated Display Engineering, Yonsei University, Seoul 03787, Republic of Korea*⁵*Wuhan University Shenzhen Institute, Shenzhen 518057, People's Republic of China*

(Received 23 October 2023; revised 25 January 2024; accepted 7 June 2024; published 31 July 2024)

Chiral organic-inorganic hybrids combining chirality of organic molecules and semiconducting properties of inorganic frameworks generate chiral excitons without external spin injection, creating the potential for chiroptoelectronics. However, the relationship between molecular chirality and exciton chirality is still unclear. Here we show the strain-amplified exciton chirality in one-dimensional chiral metal halides. Utilizing chirality-induced spin-orbital coupling theory, we quantitatively demonstrate the impact of the strain-engineered molecular assembly of chiral cations on exciton chirality, offering a feasible way to amplify exciton chirality by molecular manipulation.

DOI: [10.1103/PhysRevLett.133.056903](https://doi.org/10.1103/PhysRevLett.133.056903)

Chirality is a fundamental trait that permeates nature from spins to spiral galaxies [1,2], reflected in excited states of semiconductors as spin-polarized excitons with spin quantum number of ± 1 , widely applied in asymmetric photocatalysis [3], biomedicine [4], information encryption [5], and quantum communication [6]. In achiral semiconductors, the production of chiral excitons requires external optical or electrical spin injection [7–9]. But for chiral semiconductors, chiral excitons can be directly generated due to spin-splitting subbands caused by spatial symmetry breaking and spin-orbital coupling (SOC) [10,11]. To evaluate the exciton chirality of chiral semiconductors, the normalized dissymmetry factor (g_{CD}) ranges from -2 to 2 calculated from preferential absorption of circularly polarized light, independent of spin-selective transport and spin relaxation processes. Natural chiral semiconductors, such as some chiral organic small molecules, exhibit feeble exciton chirality (g_{CD} of 10^{-3}) due to size mismatch with electromagnetic [12]. All organic chiral polymers or supramolecules are designed to amplify exciton chirality (g_{CD} of $10^{-2} \sim 10^0$) by exciton coupling [13–15], but challenges arise from the poor carrier and exciton transport caused by disordered molecular orientation [16].

Recently, chiral organic-inorganic hybrid metal halides (CMHs) exhibited adjustable bandgap [17], long spin relaxation time [18], and highly oriented crystallization [19], and have been integrated into many spin- and

polarization-selective optoelectronic devices, ranging from polarization-selective photodetectors to spin LEDs [20–23]. However, there is a fundamental challenge of insufficient exciton chirality, which arises from chirality transfer from chiral organic molecules to metal halide frameworks. This transfer process is heavily influenced by organic-inorganic interactions, dependent on factors like composition and relative positioning of chiral organic molecules and metal halide frameworks [11,24]. Therefore, most of the experimental attempts enhanced exciton chirality by compositional and structural modifications, such as chiral molecules engineering [25–28], halide mixing [17], metal alloying [29], and manipulation of structural dimensions [30,31]. Among them, the structure and arrangement of chiral organic molecules have the most remarkable impact on exciton chirality [26,27]. However, these experimental attempts mostly demonstrated limited improvement of exciton chirality, the g_{CD} of reported CMHs typically within the range of 10^{-4} to 10^{-2} , due to the lack of understanding of the connection between molecular chirality and exciton chirality.

Herein, we unveil the relationship between the spatially helical-arranged chiral organic molecules and exciton chirality in strain-engineered one-dimensional (1D) *R*-1-(1-naphthyl)ethylammonium lead iodide (*R*-NEAPbI₃) films. Leveraging density functional theory (DFT) calculations, we show that the promotion of chiral transfer is realized by controlling molecular assembly when applying tensile strain along the in-plane direction of 1D CMH. To experimentally induce strain distribution, we introduce excess PbI₂ to 1D CMH films for introducing interfacial

*Contact author: sc.hou@whu.edu.cn

interactions. With tensile strain increasing from 0.45% to 1.50% to films, the intrinsic chiroptical response improves about 5 times, with circular dichroism (CD) and g_{CD} reaching 5400 mdeg and 0.20 respectively. We further quantitatively demonstrate the impact of helix radius and spacing of molecular assembly on exciton chirality through chirality-induced SOC theory. Based on the agreement between experimental data and theory, the maximum exciton chirality with CD of 9850 mdeg and g_{CD} of 0.35 is predictable in our case. Our study contributes to optimizing the assembly of chiral organic molecules in hybrid semiconductors toward maximum exciton chirality for chiroptoelectronic applications.

We focus on 1D R -NEAPbI₃ [32], whose soft lattice accommodates larger lattice strain than two-dimensional (2D) CMHs. This 1D CMH comprises interwoven inorganic chains ($[PbI_3]^-$) intertwined with interchain chiral ammonium cations (R -NEA⁺). These interchain molecules adopt a helical arrangement that runs vertically to the inorganic frameworks with 2₁-fold helical symmetry. R -NEA⁺ play an important role in organic-inorganic interactions and their band structures. The positive charges accumulate in ammonium of R -NEA⁺, and the negative charges accumulate in I atom of $[PbI_3]^-$ chains [Fig. 1(a)], indicating the strong electrostatic interaction between R -NEA⁺ and inorganic frameworks. The indirect bandgap of 1D CMH is shown in Fig. 1(b), its valence band maximum is completely comprised of inorganic-derived states (Pb and I atoms), whereas the conduction band minimum is mainly derived from the organic component (C atoms).

We further study the impact of molecular assembly on chiral transfer by utilizing DFT structure optimization under different strains (see the Supplemental Material [33] for details). The efficacy of chiral transfer is measured by the variation of hydrogen-bonding interactions and deformation of 1D chains [27]. There are four distinguishable hydrogen bonds surrounding an individual octahedron

$[PbI_4]^{2-}$. The difference in length of hydrogen bonds on both sides ($HB_{top-2} - HB_{top-1}$ and $HB_{bot-1} - HB_{bot-2}$) is used to assess the asymmetry of hydrogen bonding interactions (Fig. S1 [33]), which induces the chiral deformation of inorganic frameworks [11]. The deformation of 1D chains is evaluated by intraoctahedron distortions, including bond length and bond angle distortion (Δd and σ^2) [46]. As shown in Fig. 1(c), we find that $HB_{top-2} - HB_{top-1}$, $HB_{bot-1} - HB_{bot-2}$, Δd , and σ^2 all increase when applying in-plane [a-b plane in Fig. 1(a)] tensile strain. This means that in-plane tensile strain augments the asymmetry of hydrogen bonding interactions and promotes the transfer of chirality to the inorganic frameworks in 1D CMH.

Based on DFT results, we employ a multiphase interfacial interaction strategy to induce tensile strain, utilizing lattice defect, lattice misfit, and thermal expansion mismatch between two phases [47–49]. The multiphase films composed of 1D CMH and excess PbI₂ phases are produced by varying the stoichiometric composition of precursor solutions. X-ray diffraction (XRD) patterns confirm the fabricated series of films are composed of a 1D CMH phase and excess PbI₂ phase [Fig. 2(a)]. The (001) plane of the PbI₂ phase appears at 12.7°, and the content of PbI₂ is tailored from 0% to 47.7% across different preparation conditions (Fig. S2 and Table S1 [33]). Scanning electron microscope studies show that the presence of an excess PbI₂ phase results in the formation of PbI₂ nanoparticles (NPs) on both the film's surface [Figs. 2(b) and 2(c)] and within its bulk (Fig. S3 [33]). Employing grazing incident XRD and the classical $2\theta - \sin^2\phi$ method, we unveil the distribution of residual strain in films [Fig. 2(d); details shown in Supplemental Material and Table S2 [33]]. This result confirms the existence of tensile strain in 1D CMH film due to the thermal expansion mismatch between 1D CMH and glass

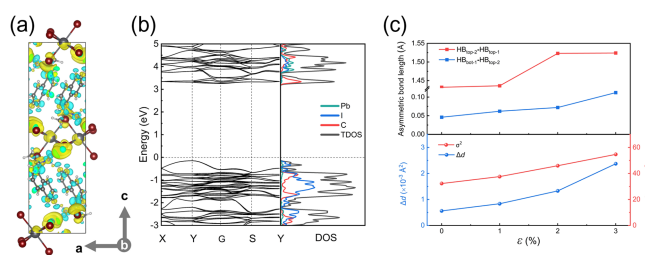


FIG. 1. Crystalline structure and band structure of 1D CMH. (a) Charge density difference image. The yellow and cyan regions represent negative charge (electron-withdrawing) and positive charge (electron-donating) respectively. (b) Band structure and density of states (DOS). There is total DOS (TDOS) and partial DOS of Pb, I, and C atoms. (c) The asymmetry of hydrogen bonding interactions ($HB_{top-2} - HB_{top-1}$ and $HB_{bot-1} - HB_{bot-2}$) and intraoctahedron distortions (Δd and σ^2) as functions of in-plane tensile strain.

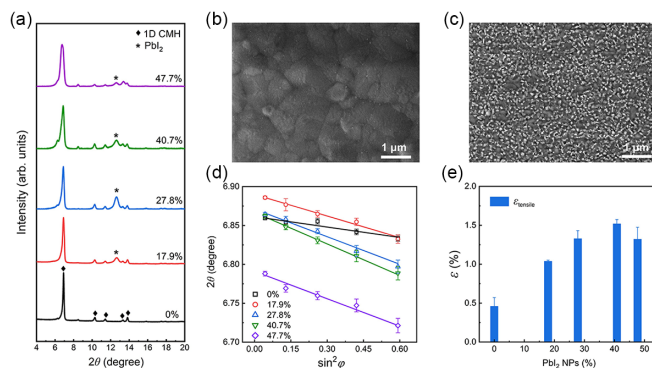


FIG. 2. Morphology and strain distribution of films. (a) XRD patterns of films with 0%, 7.9%, 27.8%, 40.7%, and 47.7% PbI₂. (b), (c) Surface morphology of 1D CMH film and multiphase film with 40.7% PbI₂. (d) Linear fitting the peak position 2θ and $\sin^2\phi$ obtains residual strain distribution. (e) The calculated tensile strain as the function of PbI₂ content.

substrate [50]. The interfacial interactions between the 1D CMH and the PbI_2 phase enhance the tensile strain in multiphase films. As such, multiphase interfacial interactions allow us to precisely tune the tensile strain from 0.45% to 1.50% by varying PbI_2 content from 0% to 40.7% [Fig. 2(e) and Fig. S4 [33]]. However, when PbI_2 content is higher than 40.7%, the agglomeration of PbI_2 NPs results in a smaller contact interface and thus reduces tensile strain (Fig. S5 [33]).

Figure 3(a) shows the absorption spectra of these films, where all exhibit an exciton absorption peak of 1D CMH at 375 nm. For multiphase films, an additional shoulder peak emerges in the absorption spectra at around 410 nm, which is attributed to the quantum confinement effect of PbI_2 NPs [40]. The contributions of 1D CMH and PbI_2 NPs to spectra are effectively separated by multipeak fitting, demonstrating the basic unchanged exciton absorption peak of 1D CMH at 375 nm (Fig. S6 [33]). From the CD spectra [Fig. 3(b)], we observe a classical opposite bisignal CD response near the exciton absorption of 1D CMH, whose peak intensity increases from 1050 mdeg to 5350 mdeg with PbI_2 content from 0% to 40.7% and then decreases beyond 40.7% PbI_2 . When the PbI_2 content further increases to 67.5%, the peak intensity of CD decreases to 200 mdeg with g_{CD} of 2.0×10^{-3} (Fig. S7 [33]). After eliminating the effects caused by the absorption overlap of PbI_2 NPs and macroscopic anisotropy of films, we calculate the true dissymmetry factor ($g_{\text{CD-TR}}$) spectra to assess intrinsic exciton chirality [Fig. 3(c); details are shown in Supplemental Material and Figs. S8–9 [33]] [42]. The $g_{\text{CD-TR}}$ has a rise of 5 times from 0% at 40.7% PbI_2 , and is also consistent with strain changes from 0.45% to 1.5%. We fail to observe any photoluminescence or circularly

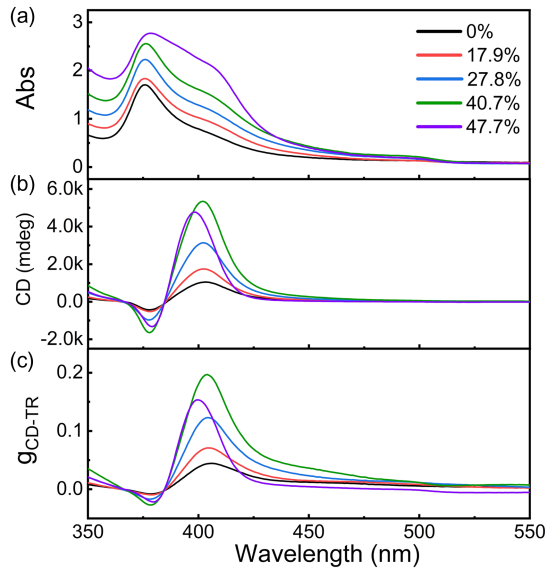


FIG. 3. The chiroptical activity of films. (a)–(c) Absorption, CD, and $g_{\text{CD-TR}}$ spectrum of 1D CMH film and multiphase films with 0%, 7.9%, 27.8%, 40.7%, and 47.7% PbI_2 .

polarized photoluminescence emission from all samples under excitation at 375 nm, which may be due to non-radiative loss channels caused by excess lattice defects, or exciton-phonon coupling caused by large lattice deformation in 1D CMH [51,52]. We further investigate the exciton dynamic and polarization dynamics by transient absorption (TA) and circularly polarized TA (CTA) spectroscopy (Figs. S10–11 [33]). 1D CMH under 1.5% strain exhibits a shorter exciton lifetime (~ 50 ps) than 1D CMH under 0.45% strain ($> 5,000$ ps), possibly due to strong exciton-phonon coupling caused by strain-induced lattice deformation, thereby aggravating the recombination of excitons [53]. Moreover, 1D CMH under 1.5% strain has the higher CTA polarization degree ($\sim 60\%$) than $\sim 20\%$ of 1D CMH under 0.45% strain, indicating the higher circular polarization degree of excitons of 1D CMH under 1.5% strain. But thermalization of excitons caused by exciton-exciton and/or exciton-phonon scattering leads to faster spin relaxation (~ 5 ps) of 1D CMH under 1.5% strain than ~ 500 ps of 1D CMH under 0.45% strain [54].

To elaborate on the relationship between molecular assembly and exciton chirality, we develop the chirality-induced SOC model for 1D CMH based on chirality-induced SOC theory [44]. This theory considers that the helical arrangement of chiral organic molecules impacts the interchain electron coupling for generating the chirality-induced SOC, which induces spin-splitting subbands and thus results in intrinsic exciton chirality. We deduce a quantitative relationship between the geometric arrangement of chiral organic molecules and the chiroptical response of CMHs, as follows (Supplemental Material [33]):

$$g_{\text{CD}} \sim \frac{\sqrt{\epsilon_b} \omega_0 D^2}{\hbar \Gamma c} \times \frac{\sin \left[\frac{\pi^3 L_d \sin \gamma}{4\pi^2 (L_d \sin \gamma + L_a \cos^2 \gamma)} \right]}{L_a^2 \cos^2 \gamma}, \quad (1)$$

where ϵ_b , \hbar , c , Γ , ω_0 , and D are the background dielectric constant, reduced Planck constant, light speed, exciton broadening, exciton resonance frequency, and exciton dipole respectively. In the latter item, molecular assembly is measured by molecular inclination (γ) along the c axis, molecular dislocation (L_d) along the a axis, and constant molecular size (L_a) (Fig. S12 [33]). The quantitative relationship demonstrates that L_d and γ contribute to higher CD and g_{CD} when other parameters are constant [Fig. 4(a)]. The molecular assembly along the c axis with 2_1 helical symmetry is regarded as a mathematically continuous helix when considering the molecular shape [55]. The helix radius (R) and spacing (H) of the molecular assembly are associated with L_d and γ by relationships of $R = 2\sqrt{L_d L_a} \sin \gamma$ and $H \approx L_a \cos \gamma / \pi$. Therefore, the enlarged radius and reduced spacing of the helix contribute to higher CD and g_{CD} , indicating that the spatially helical assembly of chiral organic molecules determines the chiral transfer process and controls the magnitude of exciton chirality.

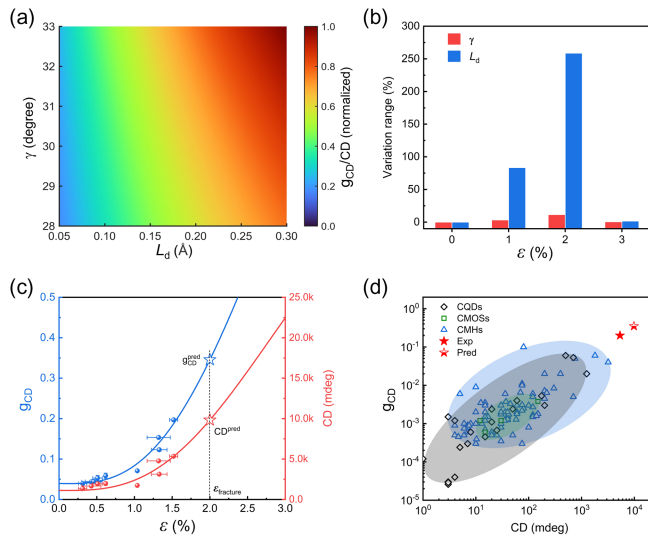


FIG. 4. The strain-amplified exciton chirality. (a) Variation of CD and g_{CD} with L_d and γ ; CD and g_{CD} are normalized. (b) Variation of L_d and γ with tensile strain. (c) The experimental g_{CD} and CD (blue and red solid points) as the function of tensile strain, well fitting with theoretical g_{CD} and CD (blue and red curves); the coefficient of determination (R^2) is 0.95 and 0.83 for g_{CD} and CD respectively. (d) Our experimental and predictable CD and g_{CD} are compared with reported CQDs, CMOSs, and CMHs.

For R -NEAPbI₃, a great increase in L_d and slight increase in γ with strain ranging from 0% to 2% [Fig. 4(b)]. The primary increase of L_d within 1%–2% strain indicates that the tensile strain effectively pulls molecules apart along the in-plane direction to enhance dislocation. L_d and γ decrease at higher strain due to the onset of tensile fracture at around 2% due to partial Pb-I bond breakage and octahedral instability. With the variation of L_d and γ under different tensile strains, we well fit experimental CD and g_{CD} according to Eq. (1) [Fig. 4(c)]. It allows us to predict a maximal CD of 9850 mdeg and g_{CD} of 0.35, at a fracture strain of about 2%. The trend of strain with exciton chirality is consistent with the results of previous studies on the electronic interactions in 2D CMHs [27]. However, different from previous studies, we clearly elucidate the impact of molecular chirality on exciton chirality, which assists us in quantitatively regulating exciton chirality through molecular manipulation. Moreover, the tunability of g_{CD} from 0.20 to 2.0×10^{-3} is higher than the reported chiral regulation strategies of CMHs (see Table S3 [33]).

In Fig. 4(d), we summarize the reported CD and g_{CD} values in three categories of chiral hybrid semiconductors, including chiral organic ligands coordinating quantum dots (CQDs), chiral metal-organic frameworks (CMOSs), and CMHs. In our work, we amplified the exciton chirality of 1D R -NEAPbI₃ and achieved a recorded CD of 5350 mdeg

and recorded g_{CD} of 0.20 among all chiral hybrid semiconductors. The highest CD and g_{CD} of 9850 mdeg and 0.35 in 1D R -NEAPbI₃ are predicted before the fracture strain, which are even comparable to chiral perovskite metasurfaces (CD = 6,350 mdeg, g_{CD} = 0.49) [56]. The high CD and g_{CD} are due to the tensile strain exerted by PbI₂ increasing the helical dislocation, thus greatly enhancing the chirality-induced SOC for amplifying exciton chirality to a recorded level.

In summary, we deduced a physical model that quantitatively describes the relationship between molecular chirality and exciton chirality. This model indicates that the spiral arrangement of chiral organic molecules with larger helix radius and smaller helix spacing results in stronger exciton chirality. The tensile strain exerted by PbI₂ greatly increased the helical dislocation of R -NEA⁺ in 1D CMH, thus amplifying the exciton chirality to the recorded level in chiral hybrid semiconductors. The phase-mixing strategy modulates the strain of 1D CMH by utilizing lattice mismatch and thermal mismatch between two phases, which has been a classic method employed in perovskite films for strain engineering [57,58]. Therefore, similar strategies are transferable for other CMHs for amplifying exciton chirality by selecting the suitable mixed phase and carefully controlling its morphology. For instance, for 2D or quasi-2D CMHs with better optoelectronic properties, whose chiral organic molecules are helically arranged between inorganic frameworks, it is desirable to adjust molecular assembly to achieve higher exciton chirality. Our work offers a feasible way to quantitatively regulate exciton chirality by molecular manipulation, fostering the advancement of chiral hybrid semiconductors, with implications across a spectrum of exciting applications in chiral light sources and detectors, chiral sensing, and asymmetric photocatalysis.

Acknowledgments—The authors thank Ziang Lu and Prof. Xiang Zhou from the College of Chemistry and Molecular Sciences of Wuhan University for their assistance on CD measurement. The authors also thank the Core Facility of Wuhan University. The authors acknowledge support from the National Natural Science Foundation of China (Grant No. 52273194), the Guangdong Basic and Applied Basic Research Foundation (Grant No. 2023A1515011642), and the Knowledge Innovation Program of Wuhan-Shuguang Project (Grant No. 2023010201020248).

S. H. supervised the research. J. X. and S. H. conceived the idea. J. X. carried out the main experiments and analyzed the data. L. F. did the DFT theoretical calculation. J. L. tested TA and CTA. J. X., H. Z., and S. H. wrote the manuscript. All authors contributed to the scientific discussion and preparation of the Letter.

The authors declare no competing interests.

- [1] M. Liu, L. Zhang, and T. Wang, Supramolecular chirality in self-assembled systems, *Chem. Rev.* **115**, 7304 (2015).
- [2] Y. Sang and M. Liu, Hierarchical self-assembly into chiral nanostructures, *Chem. Sci.* **13**, 633 (2022).
- [3] X. Kang, X. Wu, X. Han, C. Yuan, Y. Liu, and Y. Cui, Rational synthesis of interpenetrated 3D covalent organic frameworks for asymmetric photocatalysis, *Chem. Sci.* **11**, 1494 (2020).
- [4] L. Xu *et al.*, Enantiomer-dependent immunological response to chiral nanoparticles, *Nature (London)* **601**, 366 (2022).
- [5] S. Liu, X. Liu, Y. Wu, D. Zhang, Y. Wu, H. Tian, Z. Zheng, and W.-H. Zhu, Circularly polarized perovskite luminescence with dissymmetry factor up to 1.9 by soft helix bilayer device, *Matter Radiat. Extremes* **5**, 2319 (2022).
- [6] J. Yin *et al.*, Satellite-based entanglement distribution over 1200 kilometers, *Science* **356**, 1140 (2017).
- [7] J. Wang, C. Zhang, H. Liu, X. Liu, H. Guo, D. Sun, and Z. V. Vardeny, Tunable spin characteristic properties in spin valve devices based on hybrid organic–inorganic perovskites, *Adv. Mater.* **31**, 1904059 (2019).
- [8] H. J. Zhu, M. Ramsteiner, H. Kostial, M. Wassermeier, H. P. Schönherr, and K. H. Ploog, Room-temperature spin injection from Fe into GaAs, *Phys. Rev. Lett.* **87**, 016601 (2001).
- [9] K. F. Mak, K. He, J. Shan, and T. F. Heinz, Control of valley polarization in monolayer MoS₂ by optical helicity, *Nat. Nanotechnol.* **7**, 494 (2012).
- [10] J. Ahn, E. Lee, J. Tan, W. Yang, B. Kim, and J. Moon, A new class of chiral semiconductors: Chiral-organic-molecule-incorporating organic–inorganic hybrid perovskites, *Mater. Horiz.* **4**, 851 (2017).
- [11] M. K. Jana, R. Song, H. Liu, D. R. Khanal, S. M. Janke, R. Zhao, C. Liu, Z. V. Vardeny, V. Blum, and D. B. Mitzi, Organic-to-inorganic structural chirality transfer in a 2D hybrid perovskite and impact on Rashba-Dresselhaus spin-orbit coupling, *Nat. Commun.* **11**, 4699 (2020).
- [12] H. Tanaka, Y. Inoue, and T. Mori, Circularly polarized luminescence and circular dichroisms in small organic molecules: Correlation between excitation and emission dissymmetry factors, *ChemPhotoChem* **2**, 386 (2018).
- [13] J. Wade *et al.*, Natural optical activity as the origin of the large chiroptical properties in π -conjugated polymer thin films, *Nat. Commun.* **11**, 6137 (2020).
- [14] J. L. Greenfield, J. Wade, J. R. Brandt, X. Shi, T. J. Penfold, and M. J. Fuchter, Pathways to increase the dissymmetry in the interaction of chiral light and chiral molecules, *Chem. Sci.* **12**, 8589 (2021).
- [15] F. Garcia and L. Sanchez, Structural rules for the chiral supramolecular organization of OPE-based discotics: Induction of helicity and amplification of chirality, *J. Am. Chem. Soc.* **134**, 734 (2012).
- [16] P. M. Beaujuge and J. M. J. Fréchet, Molecular design and ordering effects in π -functional materials for transistor and solar cell applications, *J. Am. Chem. Soc.* **133**, 20009 (2011).
- [17] J. Ahn, S. Ma, J. Y. Kim, J. Kyhm, W. Yang, J. A. Lim, N. A. Kotov, and J. Moon, Chiral 2D organic inorganic hybrid perovskite with circular dichroism tunable over wide wavelength range, *J. Am. Chem. Soc.* **142**, 4206 (2020).
- [18] H. Lu, J. Wang, C. Xiao, X. Pan, X. Chen, R. Brunecky, J. J. Berry, K. Zhu, M. C. Beard, and Z. V. Vardeny, Spin-dependent charge transport through 2D chiral hybrid lead-iodide perovskites, *Sci. Adv.* **5**, eaay0571 (2019).
- [19] C. Chen, L. Gao, W. Gao, C. Ge, X. Du, Z. Li, Y. Yang, G. Niu, and J. Tang, Circularly polarized light detection using chiral hybrid perovskite, *Nat. Commun.* **10**, 1927 (2019).
- [20] Y.-H. Kim *et al.*, Chiral-induced spin selectivity enables a room-temperature spin light-emitting diode, *Science* **371**, 1129 (2021).
- [21] Z. Liu *et al.*, Chiral hybrid perovskite single-crystal nanowire arrays for high-performance circularly polarized light detection, *Adv. Sci.* **8**, 2102065 (2021).
- [22] J. Hao, H. Lu, L. Mao, X. Chen, M. C. Beard, and J. L. Blackburn, Direct detection of circularly polarized light using chiral copper chloride–carbon nanotube heterostructures, *ACS Nano* **15**, 7608 (2021).
- [23] K. Kim *et al.*, Chiral-phonon-activated spin Seebeck effect, *Nat. Mater.* **22**, 322 (2023).
- [24] J. Son *et al.*, Unraveling chirality transfer mechanism by structural isomer-derived hydrogen bonding interaction in 2D chiral perovskite, *Nat. Commun.* **14**, 3124 (2023).
- [25] J. Lin, D. Chen, L. Yang, T. Lin, Y. Liu, Y. Chao, P. Chou, and C. Chiu, Tuning the circular dichroism and circular polarized luminescence intensities of chiral 2D hybrid organic–inorganic perovskites through halogenation of the organic ions, *Angew. Chem. Int. Ed.* **60**, 21434 (2021).
- [26] L. Yan, M. K. Jana, P. C. Sercel, D. B. Mitzi, and W. You, Alkyl-aryl cation mixing in chiral 2D perovskites, *J. Am. Chem. Soc.* **143**, 18114 (2021).
- [27] S. Ma, Y.-K. Jung, J. Ahn, J. Kyhm, J. Tan, H. Lee, G. Jang, C. U. Lee, A. Walsh, and J. Moon, Elucidating the origin of chiroptical activity in chiral 2D perovskites through nanoconfined growth, *Nat. Commun.* **13**, 3259 (2022).
- [28] C. U. Lee *et al.*, Tailoring the time-averaged structure for polarization-sensitive chiral perovskites, *J. Am. Chem. Soc.* **144**, 16020 (2022).
- [29] H. Lu *et al.*, Highly distorted chiral two-dimensional tin iodide perovskites for spin polarized charge transport, *J. Am. Chem. Soc.* **142**, 13030 (2020).
- [30] G. K. Long *et al.*, Spin control in reduced-dimensional chiral perovskites, *Nat. Photonics* **12**, 528 (2018).
- [31] T. Liu, W. Shi, W. Tang, Z. Liu, B. C. Schroeder, O. Fenwick, and M. J. Fuchter, High responsivity circular polarized light detectors based on quasi two-dimensional chiral perovskite films, *ACS Nano* **16**, 2682 (2022).
- [32] A. Ishii and T. Miyasaka, Direct detection of circular polarized light in helical 1D perovskite-based photodiode, *Sci. Adv.* **6**, eabd3274 (2020).
- [33] See Supplemental Material at <http://link.aps.org/supplemental/10.1103/PhysRevLett.133.056903> for additional information about experimental methods, DFT calculations, and extended data, which includes Refs. [17,25–27,30,34–45].
- [34] G. Kresse and J. Hafner, Norm-conserving and ultrasoft pseudopotentials for first-row and transition elements, *J. Phys. Condens. Matter* **6**, 8245 (1994).
- [35] P. E. Blöchl, Projector augmented-wave method, *Phys. Rev. B* **50**, 17953 (1994).

- [36] J. P. Perdew, A. Ruzsinszky, G. I. Csonka, O. A. Vydrov, G. E. Scuseria, L. A. Constantin, X. Zhou, and K. Burke, Restoring the density-gradient expansion for exchange in solids and surfaces, *Phys. Rev. Lett.* **100**, 136406 (2008).
- [37] S. Grimme, J. Antony, S. Ehrlich, and H. Krieg, A consistent and accurate *ab initio* parametrization of density functional dispersion correction (DFT-D) for the 94 elements H-Pu, *J. Chem. Phys.* **132**, 154104 (2010).
- [38] H. Wang *et al.*, Interfacial residual stress relaxation in perovskite solar cells with improved stability. *Adv. Mater.* **31**, 1904408 (2019).
- [39] Z. Chen, N. Prud'homme, B. Wang, and V. Ji, Residual stress gradient analysis with GIXRD on ZrO₂ thin films deposited by MOCVD. *Surf. Coat. Technol.* **206**, 405 (2011).
- [40] G. Zhu, P. Liu, M. Hojamberdiev, J. Zhou, X. Huang, B. Feng, and R. Yang, Controllable synthesis of PbI₂ nanocrystals via a surfactant-assisted hydrothermal route, *Appl. Phys. A* **98**, 299 (2010).
- [41] M. Schulz, J. Zablocki, O. S. Abdullaeva, S. Brück, F. Balzer, A. Lützen, O. Arteaga, and M. Schiek, Giant intrinsic circular dichroism of prolinol-derived squaraine thin films, *Nat. Commun.* **9**, 2413 (2018).
- [42] Z. Zhang, Z. Wang, H. H. Y. Sung, I. D. Williams, Z. Yu, and H. Lu, Revealing the intrinsic chiroptical activity in chiral metal-halide semiconductors, *J. Am. Chem. Soc.* **144**, 22242 (2022).
- [43] S. Liu *et al.*, Bright circularly polarized photoluminescence in chiral layered hybrid lead-halide perovskites, *Sci. Adv.* **9**, eadh5083 (2023).
- [44] Z. Yu, Chirality-induced spin-orbit coupling, spin transport, and natural optical activity in hybrid organic-inorganic perovskites, *J. Phys. Chem. Lett.* **11**, 8638 (2020).
- [45] B. Yao, Q. Wei, Y. Yang, W. Zhou, X. Jiang, H. Wang, M. Ma, D. Yu, Y. Yang, and Z. Ning, Symmetry-broken 2D lead-tin mixed chiral perovskite for high asymmetry factor circularly polarized light detection, *Nano Lett.* **23**, 1938 (2023).
- [46] K. Du, Q. Tu, X. Zhang, Q. Han, J. Liu, S. Zauscher, and D. B. Mitzi, Two-dimensional lead (II) halide-based hybrid perovskites templated by acene alkylamines: Crystal structures, optical properties, and piezoelectricity, *Inorg. Chem.* **56**, 9291 (2017).
- [47] H. Zhang *et al.*, Excess PbI₂ Management via multimode supramolecular complex engineering enables high-performance perovskite solar cells, *Adv. Energy Mater.* **12**, 2201663 (2022).
- [48] T. Meier, T. P. Gujar, A. Schönleber, S. Olthof, K. Meerholz, S. van Smaalen, F. Panzer, M. Thelakkat, and A. Köhler, Impact of excess PbI₂ on the structure and the temperature dependent optical properties of methylammonium lead iodide perovskites, *J. Mater. Chem. C* **6**, 7512 (2018).
- [49] M. U. Rothmann *et al.*, Atomic-scale microstructure of metal halide perovskite, *Science* **370**, eabb5940 (2020).
- [50] D. Xue *et al.*, Regulating strain in perovskite thin films through charge-transport layers, *Nat. Commun.* **11**, 1514 (2020).
- [51] Z. Li, Y. Yan, M. Song, J. Xin, H. Wang, H. Wang, and Y. Wang, Exciton-phonon coupling of chiral one-dimensional lead-free hybrid metal halides at room temperature, *J. Phys. Chem. Lett.* **13**, 4073 (2022).
- [52] X. Wang, W. Meng, W. Liao, J. Wang, R. Xiong, and Y. Yan, Atomistic mechanism of broadband emission in metal halide perovskites, *J. Phys. Chem. Lett.* **10**, 501 (2019).
- [53] J. Ma, C. Fang, C. Chen, L. Jin, J. Wang, S. Wang, J. Tang, and D. Li, Chiral 2D perovskites with a high degree of circularly polarized photoluminescence, *ACS Nano* **13**, 3659 (2019).
- [54] T. C. Damen, K. Leo, J. Shah, and J. E. Cunningham, Spin relaxation and thermalization of excitons in GaAs quantum wells, *Appl. Phys. Lett.* **58**, 1902 (1991).
- [55] I. Hisaki, T. Sasaki, N. Tohnai, and M. Miyata, Supramolecular-tilt-chirality on twofold helical assemblies, *Chem. Eur. J.* **18**, 10066 (2012).
- [56] G. Long, G. Adamo, J. Tian, M. Klein, H. N. S. Krishnamoorthy, E. Feltri, H. Wang, and C. Soci, Perovskite metasurfaces with large superstructural chirality, *Nat. Commun.* **13**, 1551 (2022).
- [57] Y. Chen *et al.*, Strain engineering and epitaxial stabilization of halide perovskites, *Nature* **577**, 209 (2020).
- [58] J. Zhao, Y. Deng, H. Wei, X. Zheng, Z. Yu, Y. Shao, J. E. Shield, and J. Huang, Strained hybrid perovskite thin films and their impact on the intrinsic stability of perovskite solar cells, *Sci. Adv.* **3**, eaao5616 (2017).